 CMC, vol.3, no.3, pp.131-145, 2006

Multi-Scale Modelling and Simulation of Textile Reinforced Materials

G. Haasemann[1], M. Kästner[1] and V. Ulbricht[1]

Abstract: Novel textile reinforced composites provide an extremely high adaptability and allow for the development of materials whose features can be adjusted precisely to certain applications. A successful structural and material design process requires an integrated simulation of the material behavior, the estimation of the effective properties which need to be assigned to the macroscopic model and the resulting features of the component.
In this context two efficient modelling strategies - the Binary Model (Carter, Cox, and Fleck (1994)) and the Extended Finite Element Method (X-FEM) (Moës, Cloirec, Cartraud, and Remacle (2003)) - are used to model materials which exhibit a complex structure on the meso-scale. For these investigations the focus is set on composites made of glass fibers, thermoset or thermoplastic matrices and on the application of commingled thermoplastic and glass fibers. Homogenization techniques are applied to compute effective macroscopic stiffness parameters. Problems arising from a complex textile reinforcement architecture, e.g. bi- or multi-axial weft-knit, woven and braided fabrics, in combination with a high fiber volume fraction will be addressed and appropriate solutions are proposed. The obtained results are verified by experimental test data.
The macroscopic stress and strain fields in a component are used for optimization of the construction and the material layout. These distributions are computed in a global structural finite element analysis. Based on the global fiber orientation the required macroscopic material properties obtained from homogenization on the meso-scale are mapped to the model of the structural part. The configuration of the fiber-orientation and textile shear deformation in complex structural components caused by the manufacturing process is determined by a three-dimensional optical measurement system.

keyword: composite materials, multi-scale, X-FEM, Binary Model, homogenization

[1] TU Dresden, Dresden, Germany

1 Introduction

Modelling structural parts made from composites requires adequate knowledge on the macroscopic behavior of the locally heterogenous material. Due to the difference in size between the macroscopic component on the one hand and the structure of the material on the other hand a direct modelling of the meso-structure in a structural analysis is not reasonable.
The computational homogenization method is an efficient solution to this problem as effective macroscopic material properties can be computed from a characteristic section of a complex structured composite.
While the application of this technique to the linear elastic case is rather simple a non-linear material behavior on the micro-scale complicates the prediction of effective properties as an appropriate macroscopic constitutive model is required. In section 2.1 the computational multi-scale homogenization is presented as an alternative approach.
The derivation of the macroscopic material properties based on a representative volume element (RVE) model is indispensable. Regarding simple structured reinforcement an analytical approach such as proposed in Kwon and Roach (2004) can be used to estimate these properties. However the complex meso-structure considered here requires numerical procedures which result in an extensive modelling effort. Moreover, sophisticated geometries involve highly distorted elements that might cause numerically ill-conditioned systems of equation. Therefore, efficient strategies are necessary in order to reduce the modelling effort significantly. Recently developed local meshless methods proposed e.g. by Atluri and Shen (2005) and Sladek, Sladek, and Tanaka (2005) can be adapted for application to these materials. For most of these procedures new computational data process and solution routines need to be developed. To avoid this requirement the Binary Model and the Extended Finite Element Method (X-FEM) are considered in this work. Both modelling strategies can be realized by extending an existing FE-program.

After a brief overview on the essential features of both methods in section 3 they are applied to composite modelling. To this end an automatic modelling procedure for the X-FEM is presented. Furthermore, a multi-scale analysis simulating a tensile test demonstrates the practicability of the multi-scale homogenization. Finally, the presented methods are utilized to design a composite bucket.

2 Materials

The remarkable advantages of pure knitted fabrics are formability and drapability, choice of net-shape fabrics and coherency of fibers. However, the disadvantage of composites with knitted fabric reinforcement is their moderate stiffness and strength. To improve these properties, a laid-in non-knitted yarn system is integrated into the knitted fabric such as illustrated in Fig. 1. According to Diestel, Haasemann, and Orawattanasrikul (2004) this novel textile structure is called biaxial weft-knitted fabric. The reinforcement used for these investigations is made of glass fibers. In general, there are no restrictions to use other materials, e.g. carbon-fibers.

To take advantage of the biaxial weft-knitted fabric and shaped parts like the elevator bucket described in section 4.3.

A second type of materials considered is a reinforcing structure made from continuous commingled yarns. Such a reinforcement consists of mechanically combined reinforcing fibers and such spun from a thermoplastic matrix. From the variety of different reinforcement and matrix materials the combination glass and polypropylene is chosen. The very flexible commingled yarns can be processed to more complex reinforcing structures such as woven fabrics. For manufacturing components the fabric is laid in a heated mould. During a compression moulding process the thermoplastic fiber is melted and constitutes the matrix after consolidation.

The computation of macroscopic material properties requires the geometric data describing the topology of the composite. For this, parameters of the filament yarn and the textile processing are used. Since a transparent matrix material is used, the in-plane geometry can be quantified with pictures obtained by optical scans. To investigate the out-of-plane geometry, spatial data of the Computer Tomography (CT) scanning provides sufficient information. The CT picture in Fig. 2 shows a section of a composite material reinforced with a glass-fiber fabric.

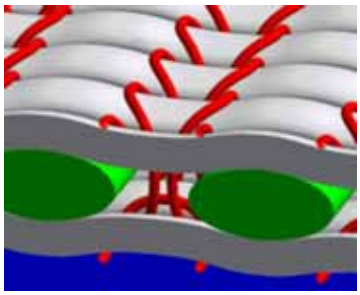

Figure 1 : Biaxial weft-knitted fabric

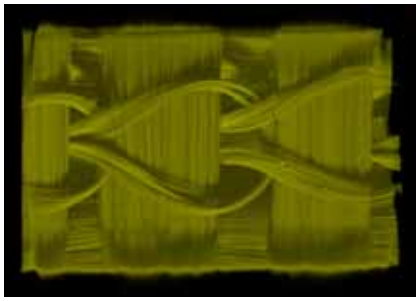

Figure 2 : CT-scan

to achieve a near-net-shaped preform, the textile is subjected to drape deformation. Up to a certain limit, this deformation is dominated by shearing and a change in the thickness of the fabric. Since deformations are not constant in a structural part, only a locally homogeneous macrostructure can be assumed. Furthermore, the material properties become highly anisotropic.

The textile fabric is consolidated with epoxy resin. Here, this is achieved by two different technologies: (i) the Resin Transfer Moulding (RTM) to produce composite plates used for experimental investigations and (ii) the vacuum injection which is applied to more complex

2.1 Homogenization

The simulation of the stress and strain fields in structural parts demands that the macroscopic material properties are known. Due to the wide range of available composite materials, including different reinforcing structures and processing technologies, the experimental estimation of these parameters becomes very expensive and time-consuming. Analytical methods can be applied to simple structured composites such as uni- or bi-directional reinforced materials. However, the computational homogenization method based on a RVE or unit cell is an

efficient strategy to obtain effective material properties and information on the local stress and strain fields of complex structured composites. There are different approaches and mathematical foundations of these methods, e.g. asymptotic homogenization (Holmbom, Persson, and Svanstedt (1991)) and the energy averaging theorem (Hill (1972)). The work here is related to the latter and some details are given in Section 2.2.

The concept of the RVE can be applied to random structures. If there is at least a locally periodic micro-structure which is the case for the composite considered in this work the RVE conforms to a unit cell of this structure. One or a set of these periodic elements can be used to define the domain V of a unit cell. Regarding the definition of boundary conditions the surface of the cell domain ∂V is subdivided into $\partial V^+ \cup \partial V^-$ in the way that two associated locations $\mathbf{x}^+ \in \partial V^+$ and $\mathbf{x}^- \in \partial V^-$, respectively, have the unit outward normal relation $\mathbf{n}^+ = -\mathbf{n}^-$.

The micro-structural deformation field of this domain will be described by $\varepsilon_{ij} := u_{(i,j)}(\mathbf{x},t)$ where u_i denotes the displacement field which depends on the material point $\mathbf{x} \in V$ and the time t. The brackets enclosing the indices represent a symmetry operator. The unit cell is in a state of equilibrium. This can be mathematically expressed in terms of the symmetric stress tensor $\boldsymbol{\sigma}$ according to

$$\sigma_{ij,i} = 0 \quad \text{and} \quad \sigma_{ij} = \sigma_{ji} \quad \text{in} \quad V \quad . \tag{1}$$

The elastic constitutive equations

$$\boldsymbol{\sigma} = F_\sigma(\boldsymbol{\varepsilon}, \mathbf{x}) \tag{2}$$

specify the stress-strain relationship. Since the composite structure is divided into N subregions of different materials such as matrix and fibers, N sets of constitutive relations are required.

Once the microscopic material behavior becomes nonlinear, the prediction of the macroscopic properties requires a definition of an appropriate constitutive model. In general it is extremely difficult to obtain a reasonable macroscopic reflection of the microscopic properties. An alternative approach which has been developed for instance by Miehe and Koch (2002) is the computational multi-scale homogenization. There is a number of different variations on the details of this procedure. However, the fundamental principle is the transition of the micro-structural response to the macroscopic structure based on the formulation of an adequate boundary value problem. The procedure outlined in this paper is illustrated in Fig. 3. At first there is a model representing a structural part and the boundary conditions. The macroscopic tangent stiffness is initialized with the linear elastic properties quantified by the homogenization procedure. Next, a load step is applied followed by the first solution. The strain obtained on the macroscopic FE-model after each iterative step is applied to the unit cell. The response in terms of the macro-stress $\boldsymbol{\Sigma}$ and the tangent stiffness $\mathbf{C}^M$ is determined. The next increment in the macroscopic computation can be applied if the solution has converged. The numerical implementation is based on the commercial FE-program ANSYS. A Fortran95 FE-subroutine has been developed to simulate the microscopic behavior of the unit cell based on the Binary Model which is outlined in section 3.1. Besides the physically and geometrically non-linear FE-solution in the framework of a small strain formulation, this routine computes the macroscopic stress and tangent stiffness. The "User Programmable Features" (UPF) (Ansys (2004)) provided by ANSYS enable the linking of this subroutine to the macroscopic model.

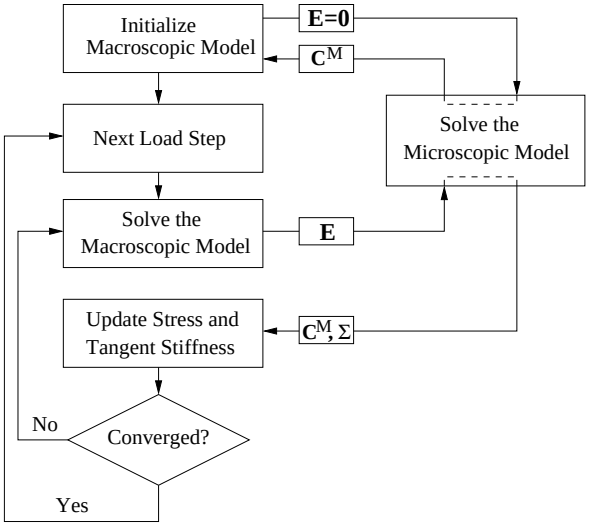

Figure 3 : Flowchart of the multi-scale procedure

Subsequently, details are given to the homogenization procedure.

2.2 Micro-to-macro transition and boundary conditions

A basic principle of this homogenization method is the micro-to-macro transition based on the unweighted volume averaging theorem. In the following this is applied

to stress, strain and stress work of the heterogeneous solid to obtain the corresponding overall quantities. The volume average is denoted by

$$\langle \cdots \rangle := \frac{1}{V} \int_{\Omega} \cdots d\Omega \tag{3}$$

Applying this to the variable stress field $\sigma(\mathbf{x})$, the macroscopic stress can be expressed as

$$\Sigma_{ij} := \langle \sigma_{ij} \rangle = \frac{1}{V} \int_{\partial V} x_i t_j dO \quad . \tag{4}$$

Eq. 4 shows that Σ_{ij} is completely defined by the microscopic stress field on the unit cell surface. Assuming that the surface tractions t_i are self-equilibrating, it can be shown that the stress defined in Eq. 4 is symmetric.
The macroscopic strain $\mathbf{E}$ is defined by the corresponding heterogeneous quantity. Applying the Gauss theorem gives

$$E_{ij} := \langle \varepsilon_{ij} \rangle = \frac{1}{V} \int_{\partial V} u_i n_j dO \quad , \tag{5}$$

where n_j denotes the unit outward normal defined at $\mathbf{x} \in \partial V$. Here again, the macroscopic strain tensor $\mathbf{E}$ is described by the microscopic displacement field on the unit cell surface only.
Finally it is observed that the local stress work is

$$\sigma_{ij}\varepsilon_{ij} = (\sigma_{ij}u_i)_{,j} - \sigma_{ij,j}u_i \tag{6}$$

In view of Eq. 1, the average stress work is given by

$$\langle \sigma_{ij}\varepsilon_{ij} \rangle = \frac{1}{V} \int_{\partial V} t_i u_i dO \quad . \tag{7}$$

In general, there are three different boundary condition under which the identity, also known as HILL-MANDEL-Lemma,

$$\langle \sigma_{ij}\varepsilon_{ij} \rangle = \langle \sigma_{ij} \rangle \langle \varepsilon_{ij} \rangle \tag{8}$$

holds: (i) linear displacements, (ii) constant tractions and (iii) a periodic displacement field added to the linear displacements and antiperiodic tractions. In the following, the last case will be denoted by "periodic displacements" or "periodic boundary conditions", only.
In the first case the displacement boundary conditions are given by

$$u_i(\mathbf{x}) = E_{ij}x_j \quad \forall \quad x_j \in \partial V, \tag{9}$$

which represent a linear deformation of the unit cell.
The constant tractions are prescribed by

$$t_i = \Sigma_{ij} n_j(\mathbf{x}) \qquad \forall \quad \mathbf{x} \in \partial V. \tag{10}$$

At last the periodic boundary condition and antiperiodic tractions are written as

$$\begin{aligned} u_i(\mathbf{x}^+) - u_i(\mathbf{x}^-) &= E_{ij}(x_j^+ - x_j^-) \quad \text{and} \\ t_i(\mathbf{x}^+) + t_i(\mathbf{x}^-) &= 0 \end{aligned} \tag{11}$$

Assuming that the shape of the unit cell is defined properly which means that the assembled structure does not have any gaps or overlay the dimension of the unit cell regarding a particular direction α is constant according to

$$\Delta x_i^{\alpha} := x_i^+ - x_i^- \quad . \tag{12}$$

Then the periodic boundary condition Eq. 11 can be written in the form

$$\Delta u_i^{\alpha} := u_i(\mathbf{x}^+) - u_i(\mathbf{x}^-) = E_{ij}\Delta x_j^{\alpha} \tag{13}$$

where Δu_i^{α} represent displacement increments which depend on the considered surface α, only. In view of an 3D unit cell, the boundary value problem requires 9 values of Δu_i^{α}. Introducing the definition of an integral surface force F_i^{α} such that

$$F_i^{\alpha} := \int_{\partial V^{\alpha}} t_i^+ dO \tag{14}$$

the macroscopic stress can be recast into the form

$$\Sigma_{ij} = \frac{1}{V} \sum_{\alpha} \Delta x_i^{\alpha} F_j^{\alpha} \quad . \tag{15}$$

Many parts made of textile reinforced composites such as the elevator bucket can be considered as shell structures in the framework of a plain stress formulation. To obtain the macroscopic quantities which are related to the plain stress state, a combination of two boundary conditions described before is used. Assuming that the orientation of the coordinate x_3 is normal to the surface, periodic boundary conditions are applied to the in-plane directions. A constant traction $t_i^{(3)} = 0$ is specified for the out-of-plane surfaces. Finally the non-zero macroscopic stress quantities are computed by Eq. 15 and the strain E_{33} is evaluated by Eq. 5.
In this paper, the homogenization procedure is focused on two formulations of the microscopic boundary conditions: (i) 3D homogenization with periodic displacements and (ii) 2D homogenization with in-plane periodic displacements and out-of-plane constant tractions.

2.3 Finite element formulation

Regarding the computational multi-scale method there are no restrictions on the modelling strategies such as the X-FEM or the Binary Model which is used for the unit cell. In the following some details on the implementation of the boundary conditions into the FE-procedure are given. Here it is assumed that all degrees of freedom of the FE-model are displacements. Then the variational global displacement vector $\delta\mathbf{u}$ and the vector of external forces $\delta\mathbf{f}$ can be structured such that

$$\delta\mathbf{u} = \begin{bmatrix} \delta\mathbf{u}^a \\ \delta\mathbf{u}^r \\ \delta\mathbf{u}^l \\ \delta\mathbf{u}^\alpha \end{bmatrix} \quad \text{and} \quad \delta\mathbf{f} = \begin{bmatrix} \mathbf{0} \\ \delta\mathbf{f}^r \\ \delta\mathbf{f}^l \\ \mathbf{0} \end{bmatrix} \tag{16}$$

where the superscripts r and l denote the quantities of surface nodes located at ∂V^+ and ∂V^-, respectively, a -all remaining nodes and α refers to additional degrees of freedom where three are defined to each surface α to which periodic displacements are assigned. Then the variational displacements $\delta\mathbf{u}^\alpha$ correspond to the increments Δu_i^α defined in Eq. 13 in the way that

$$\delta u_i^\alpha := \delta E_{ij} \Delta x_j^\alpha \quad , \tag{17}$$

where Δ in $\delta\Delta u_i^\alpha \equiv \delta u_i^\alpha$ is dropped for notational brevity. Let the matrix $\mathbf{K}$ represent a linear transformation relative to $\delta\mathbf{u}$ and $\delta\mathbf{f}$, it can be partitioned in the same manner such that

$$\mathbf{K} = \begin{bmatrix} \mathbf{K}^{aa} & \mathbf{K}^{ar} & \mathbf{K}^{al} & \mathbf{0} \\ \mathbf{K}^{ra} & \mathbf{K}^{rr} & \mathbf{K}^{rl} & \mathbf{0} \\ \mathbf{K}^{la} & \mathbf{K}^{lr} & \mathbf{K}^{ll} & \mathbf{0} \\ \mathbf{0} & \mathbf{0} & \mathbf{0} & \mathbf{0} \end{bmatrix} \tag{18}$$

Based on the periodic boundary conditions Eq. 13, the displacements $\delta\mathbf{u}^r$ can be expressed depending on $\delta\mathbf{u}^l$ and $\delta\mathbf{u}^\alpha$. The incorporation of this relation leads to the transformation $\delta\mathbf{u} = \mathbf{T}\delta\tilde{\mathbf{u}}$ with:

$$\delta\tilde{\mathbf{u}} = \begin{bmatrix} \delta\mathbf{u}^a \\ \delta\mathbf{u}^l \\ \delta\mathbf{u}^\alpha \end{bmatrix} \quad \text{and} \quad \mathbf{T} = \begin{bmatrix} \mathbf{I} & \mathbf{0} & \mathbf{0} \\ \mathbf{0} & \mathbb{C} & \mathbb{D} \\ \mathbf{0} & \mathbf{I} & \mathbf{0} \\ \mathbf{0} & \mathbf{0} & \mathbf{I} \end{bmatrix} \quad , \tag{19}$$

where $\mathbf{I}$ is the identity matrix. The matrices $\mathbb{C}$ and $\mathbb{D}$ represent the discretized coupling constraints according to Eq. 13 and are filled with one and zero, only. The standard elimination procedure of the dependent quantities leads to the system

$$\left[\mathbf{T}^T\mathbf{K}\mathbf{T}\right]\delta\tilde{\mathbf{u}} = \begin{bmatrix} \mathbf{0} \\ \mathbb{C}^T\delta\mathbf{f}^r + \delta\mathbf{f}^l \\ \mathbb{D}^T\delta\mathbf{f}^r \end{bmatrix} =: \begin{bmatrix} \mathbf{0} \\ \delta\tilde{\mathbf{f}}^r \\ \delta\mathbf{f}^\alpha \end{bmatrix} \quad . \tag{20}$$

Considering the structure of the matrices $\mathbb{C}$ and $\mathbb{D}$ regarding the nodes which are not located at edges or corners of the unit cell, the external forces can be evaluated by the expressions $\delta\tilde{\mathbf{f}}^r = \delta\mathbf{f}^l + \delta\mathbf{f}^r$ and $\delta\mathbf{f}^\alpha = \sum\delta\mathbf{f}^r$. The degrees of freedom originated by nodes located at edges and corners requires further examinations which are not outlined here. However, this does not affect the following conclusions. To meet the condition of anti-periodic tractions given in Eq. 11b : $\delta\tilde{\mathbf{f}}^r = \mathbf{0}$. The interpretation of the external forces $\delta\mathbf{f}^\alpha$ results in the correlation to the integral surface forces F_i^α defined in Eq. 14. Then, the evaluation of Eq. 15 gives the variational macroscopic stress based on the forces acting on the additional degree of freedom and the dimension of the unit cell. Note that there are no restrictions on the general shape of the unit cell except for these mentioned in section 2.2.

2.4 Tangent stiffness

An essential procedure of the multi-scale method is the computation of the macroscopic tangent stiffness. There is a number of different solutions proposed to this problem (Miehe and Koch (2002); Kouznetsova (2002)). In the following, two approaches will be outlined and compared.

The first, for instance used by Kouznetsova (2002), is based on a condensation of the microscopic to the macroscopic stiffness. For this procedure, Eq. 20 is partitioned according to

$$\begin{bmatrix} \tilde{\mathbf{K}}^{dd} & \tilde{\mathbf{K}}^{d\alpha} \\ \tilde{\mathbf{K}}^{\alpha d} & \tilde{\mathbf{K}}^{\alpha\alpha} \end{bmatrix} \begin{bmatrix} \delta\mathbf{u}^d \\ \delta\mathbf{u}^\alpha \end{bmatrix} = \begin{bmatrix} \mathbf{0} \\ \delta\mathbf{f}^\alpha \end{bmatrix} \quad . \tag{21}$$

Except for the additional degrees of freedom, the index d refers to all remaining degrees of freedom covered by Eq. 20. A reduced stiffness matrix can be defined by

$$\mathbf{K}^M\delta\mathbf{u}^\alpha = \delta\mathbf{f}^\alpha \quad \text{with}$$
$$\mathbf{K}^M = \tilde{\mathbf{K}}^{\alpha\alpha} - \tilde{\mathbf{K}}^{\alpha d}(\tilde{\mathbf{K}}^{dd})^{-1}\tilde{\mathbf{K}}^{d\alpha} \quad . \tag{22}$$

Let the matrix $\mathbb{B}$ denote a transformation such that $\delta u_i^\alpha = \mathbb{B}_{ij}\delta\overline{E}_j$, where $\delta\overline{E}_j$ is a matrix representation of δE_{ij},

then the macroscopic tangent stiffness is obtained by

$$\mathbf{C}^M = \frac{1}{V}\mathbb{B}^T\mathbf{K}^M\mathbb{B} \quad . \tag{23}$$

A second approach will be introduced here. Since the transformation between $\delta\mathbf{u}^\alpha$ and $\delta\mathbf{f}^\alpha$ is completely given in Eq. 21, a number of $n(i,j)$ unit strains

$$\Delta u_i^\alpha := E^n \Delta x_j^{(\alpha)} \quad \text{with} \quad E^n := E_{ij} = 1$$

$$\Delta u_k^\alpha := 0 \qquad \forall \quad k \neq i \tag{24}$$

are assigned to the FE-system, successively. The relation between n and i,j is given in Tab. 1. Then, the linear

Table 1 : $n(i,j)$

n	1	2	3	4	5	6
i	1	2	1	3	1	2
j	1	2	2	3	3	3

system of equations needs to be solved for $n = \{1,2,3\}$ or $n = \{1,\ldots,6\}$ in the case of a 2D or 3D homogenization, respectively. The resulting forces $\Delta\mathbf{f}^\alpha$ at the additional nodes are used to compute the macroscopic stresses by Eq. 15. These quantities correspond to the tangent stiffness elements in $\mathbf{C}^M$ which relate the assigned unit strains to the stresses in the macroscopic constitutive equations.

Although the second procedure requires a number of solutions of the entire system, there are the following advantages: (i) the FE stiffness matrix does not need to be restructured according to Eq. 21 and (ii) there is no need on the computation of an inverse matrix which is a crucial part of the first procedure. It is observed that the second procedure can be faster up to 40% since especially for large models representing the unit cell the computation of the inverse matrix is very time-consuming.

3 MODELLING STRATEGIES

Modelling composite materials with a complex reinforcing structure on the meso-scale causes an extensive meshing effort if the ordinary finite element method is used. Subsequently, in order to ease this process two efficient modelling strategies will be presented.

3.1 The Binary Model

As proposed in literature (Carter, Cox, and Fleck (1994); Carter, Cox, McGlockton, and Xu (1995)), the Binary Model was used to predict the mechanical properties of composites with interlock weaves. Considering the complex geometry of the reinforcing weft-knitted fabric, less modelling and computational effort is needed compared to a FE-Model of volume elements, only. The Binary Model is subdivided into tows which represent the axial stiffness of yarns and the effective medium which represents the transverse and shear stiffness and the Poisson's effect of the composite. In the FE-model, tows and effective medium are replaced by two-noded line and 8-node volume elements, respectively.

Based on the geometric data obtained in section 2, a FE-mesh representing a unit cell is generated. An example is shown in Fig. 4.

As described in section 2, the textile reinforcement is

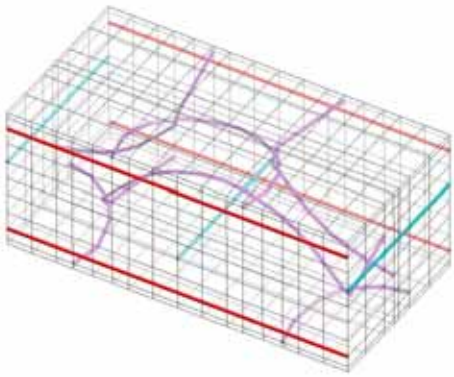

Figure 4 : FE-mesh of a unit cell

subjected to in-plane shear deformation if e.g. the shape of the structural part features double-curved surfaces. To determine the architecture of the unit cells, it is supposed that there is a kinematic shear deformation, only. Consequently the deformation due to a shear angle γ can be expressed by

$$\begin{bmatrix} x_1 \\ x_2 \end{bmatrix} = \begin{bmatrix} 1 & \sin\gamma \\ 0 & \cos\gamma \end{bmatrix} \begin{bmatrix} X_1 \\ X_2 \end{bmatrix} \quad , \tag{25}$$

where X_i and x_i are the coordinates of the original and the deformed unit cell, respectively. In general, this transformation can be applied to all geometric parameters representing the cell geometry. This requires the generation of a new mesh to each new shear angle. In view

of a procedure which computes the macroscopic material properties automatically, this is not an adequate approach. However, a transformation based on Eq. 25 of nodal coordinates in an existing mesh gives a solution to this problem.
The elastic parameters of the tow and effective medium elements are estimated by analytical models of unidirectional and biaxial composites as proposed in Carter, Cox, McGlockton, and Xu (1995). Furthermore, the failure strain of the matrix material is incorporated to determine nonlinear elastic properties.

3.2 The Extended Finite Element Method

Based on the partition of unity technique (Melenk and Babuška (1996)) the X-FEM offers the possibility to model arbitrary discontinuities using regular finite element meshes that do not need to match boundary layers.

3.2.1 Fundamentals

Modelling the mechanical behavior at interfaces which are now allowed to intersect elements is realized by local enrichment of the displacement approximation

$$\mathbf{u}^{\text{X-FEM}} = \sum_i N_i \left(\mathbf{u}_i + \mathbf{a}_i F\right) \quad . \tag{26}$$

For that purpose additional degrees of freedom $\mathbf{a}_i$ are introduced at nodes whose support is cut by an interface (Fig. 5 (a)). These degrees of freedom are weighted by an enrichment function F that accounts for the character of the interface. N_i are ordinary finite element shape functions and $\mathbf{u}_i$ degrees of freedom representing the displacement at element node i. Discontinuities in the approximated field variable as well as its partial derivatives are accounted for by suitable enrichment functions Belytschko, Moës, Usui, and Parimi (2001).
In recent years this method was applied to a variety of problems including crack modelling (Belytschko and Black (1999)), crack growth (Moës, Dolbow, and Belytschko (1999)) as well as material interfaces (Moës, Cloirec, Cartraud, and Remacle (2003)).
In addition to appropriate enrichment functions for modelling the mechanical behavior at an interface a successful implementation of the X-FEM requires a reasonable feature to localize interfaces in a regular and nonconforming finite element mesh. The so called level-set-method can be used to track the location of a given interface in the mesh. In this context the term level-set labels

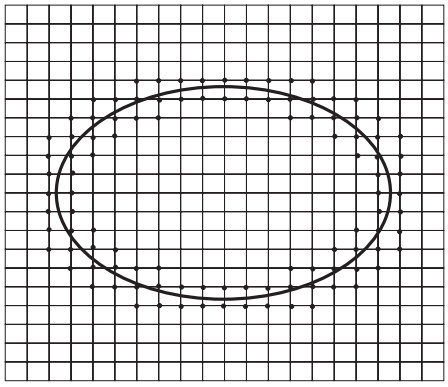

(a) Nodes with additional degrees of freedom

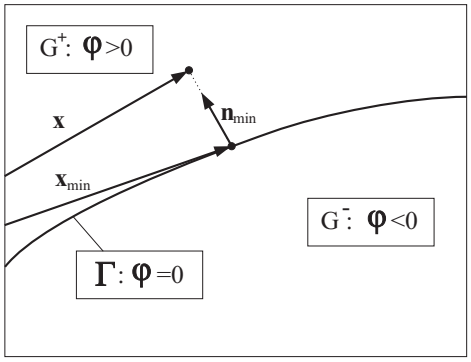

(b) Illustration to the level-set-method

Figure 5 : Enriched nodes and level-set-method

a parameter curve or surface

$$\varphi(\mathbf{x},t) = c \quad . \tag{27}$$

The variables $\mathbf{x}$ and t indicate that the function φ can depend on space and time which allows for tracking of moving interfaces.
If $c = 0$ and the level-set-function φ is chosen as a signed distance function

$$\varphi(\mathbf{x}) = (\mathbf{x} - \mathbf{x}_{min}) \cdot \mathbf{n}_{min} \tag{28}$$

the location of the fixed interface Γ is given by $\varphi = 0$ where $\mathbf{x}_{min}$ is the position vector of the point on the interface with the minimum distance to the considered point at $\mathbf{x}$ and $\mathbf{n}_{min}$ is the associate normal unit vector. According to Fig. 5 (b) values larger than zero are assigned to points in a region G^+, while points in G^- yield values less than zero

$$\varphi \begin{cases} = 0 & \text{on } \Gamma \quad ; \\ < 0 & \text{in } G^- \quad ; \\ > 0 & \text{in } G^+ \quad . \end{cases} \tag{29}$$

In a finite element mesh values of the level-set-function are only computed at nodes. Its distribution in the domain is then interpolated using the standard shape functions

$$\varphi(\mathbf{x}) = \sum_i N_i \varphi_i \quad . \tag{30}$$

Due to this interpolation which limits the accuracy of the interface approximation the mesh has to be sufficiently refined in order to locate an interface precisely.

3.2.2 Enrichment function for material interfaces

The level-set-function is of particular importance for the formulation of enrichment functions. If the governing equations of the linear elastic field problem are written as

$$\sigma_{kl,k} + f_l = 0, \sigma_{kl} = \sigma_{lk} \tag{31}$$

$$\varepsilon_{kl} = \frac{1}{2}(u_{k,l} + u_{l,k}) \tag{32}$$

$$\sigma_{kl} = C_{klmn}\varepsilon_{mn} \tag{33}$$

a sudden change of the coefficients C_{klmn} in Eq. 33 occurs at material interfaces. This implicates a discontinuity of stress and strain distributions perpendicular to the interface.

Looking at the interpolated values of the level-set-function in an element (Fig. 6) it can be seen that the function itself and its first partial derivatives are continuous over the interface.

Using the absolute value of the level-set-interpolation as shown in Fig. 7 (a) is a smart way to introduce the desired discontinuity (Sukumar, Chopp, Moës, and Belytschko (2001))

$$\tilde{F}(\varphi(\mathbf{x})) = \left| \sum_i N_i \varphi_i \right| \quad . \tag{34}$$

On the other hand it can be seen that the influence of the enrichment function $\tilde{F}$ is not limited to the region of a single element which is unfavorable for the definition of a special extended finite element that is to be used together with standard elements in the same mesh. In that case an enrichment function that is zero at element boundaries

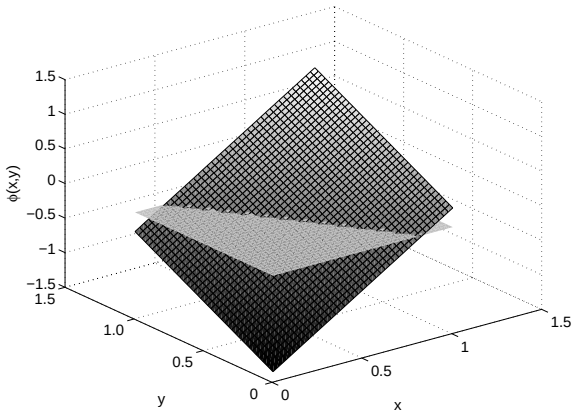

Figure 6 : Interpolation of the level-set-function in an element domain

connected to standard elements is desired. This can be ensured by choosing the enrichment function

$$F(\varphi(\mathbf{x})) = \sum_i N_i |\varphi_i| - \left| \sum_i N_i \varphi_i \right| \tag{35}$$

as suggested in Moës, Cloirec, Cartraud, and Remacle (2003) (Fig. 7 (b)).

3.2.3 Implementation

Since extending an existing program system has the clear advantage that powerful pre-, post-processing and solution procedures can be used the practical realization is performed in MARC/MENTAT using the user-subroutine feature. Nevertheless, this also poses some limitations to the flexibility of the code.

Here a special extended finite element (x-element) is defined and integrated into the course of computations in MARC which is illustrated in Fig. 8 (a). The user-subroutine is called during the assembly of the global stiffness matrix and computes element stiffness matrices for all x-elements in the mesh which are then transfered to MARC. In addition, the routine accomplishes the gradient recovery for the new element type. This user-defined element replaces original finite elements in a domain that is intersected by an interface as it is shown in Fig. 8 (b).

Essential data such as material properties, location of the interface in each element defined by the level-set-function values φ_i at nodes, etc. is obtained during pre-processing.

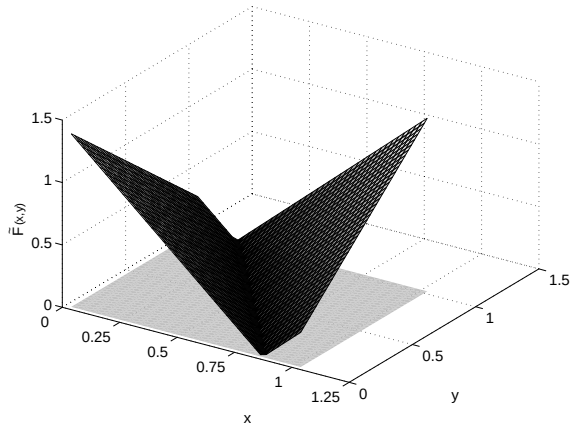

(a) $\tilde{F}(\mathbf{x})$

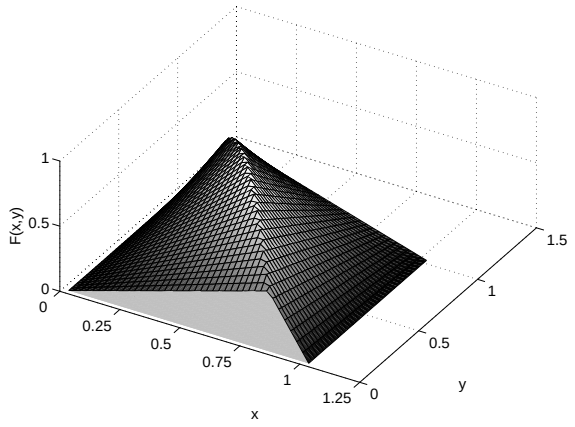

(b) $F(\mathbf{x})$

Figure 7 : Enrichment function in an element domain intersected by a material interface

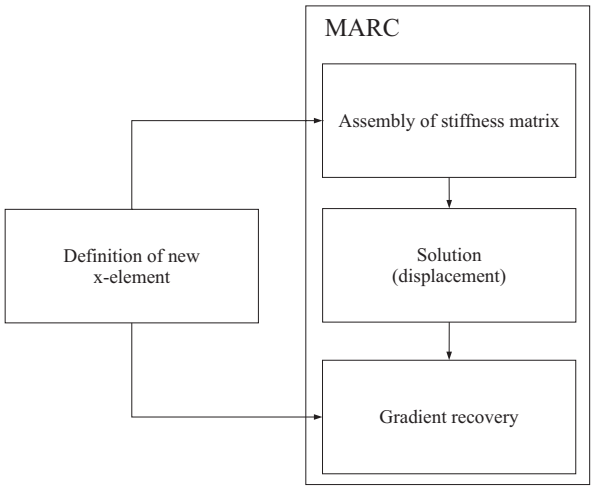

(a) Implementation of user-defined elements in MARC

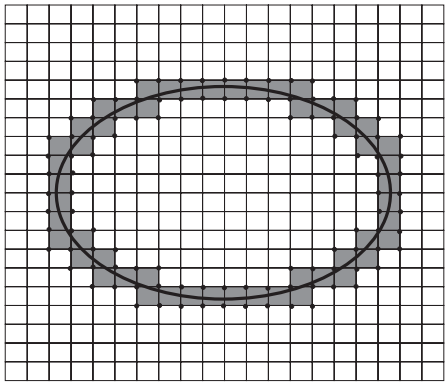

(b) X-elements in a regular X-FEM mesh

Figure 8 : Implementation of the X-FEM

Based on this information the integration of the element stiffness matrix

$$\mathbf{K}^e = \int_{\Omega_e} \mathbf{B}^T \mathbf{D}\,(C_{klmn})\,\mathbf{B}\,d\Omega_e \tag{36}$$

is performed where **D** denotes a matrix notation of C_{ijkl} acting between the stress and strain vector typical for finite element formulations. Due to the enrichment the integrand and more precisely the matrix **B**, that contains partial derivatives of shape and enrichment functions, is discontinuous over the interface Γ. Therefore, the element is divided into integration sub-domains Ω_s applying DELAUNAY triangulation in the two-dimensional case or hex-tet subdivision in three dimensions respectively

$$\int d\Omega_e \;\Rightarrow\; \sum_s \int d\Omega_s \quad . \tag{37}$$

4 APPLICATION TO COMPOSITES

4.1 X-FEM

As it was mentioned in 3.2 the major benefits of X-FEM like regular meshes and reduced meshing effort while retaining all advantages of the finite element approach have been demonstrated recently. However, changing from academic examples to practical tasks raises new questions and problems. During the application to composite materials with a considerably complex reinforcing structure on the meso-scale two key aspects can be identified. Due to the complex geometry an analytical description

of the material interface is virtually impossible. Hence, computation of level-set-values is more difficult as discrete representations of the interface might lead to ambiguous results. In addition, the model of a RVE generally includes multiple fibers which necessitates several sets of level-set-functions and extensive computations.
Furthermore, even on a meso-scale level yarns exhibit in general an anisotropic material behavior. Given that the yarn consists of isotropic fibers a transverse isotropic material behavior is common. Regarding woven fabrics a variable orientation has to be considered.
These topics are to be handled by an automated model generation algorithm.

4.1.1 Automated Model Generation

It was stated above that due to the complexity of the reinforcement structure a closed analytic description of the interface is hardly possibly. Hence, a discrete representation of the material interfaces in the considered domain is needed. Since the layout of the reinforcement is often imported from CAD systems a connection between level-set-method and CAD geometries has to be established. For this reason the following general outline of an automated model or mesh generation procedure is proposed.
The starting point is a solid volume model of the reinforcing structure such as in Fig. 9 (a). MARC/MENTAT offers a variety of interfaces to import geometry models for that purpose.
In a second step a regular X-FEM mesh which is fine enough to approximate the internal material boundaries in a sufficient way is defined and superposed to the reinforcement geometry.
Now, for each element it is checked if the element intersects any of the defined fiber volumes using boolean operations and appropriate case differentiation. The result for a demonstrative example taken from Moës, Cloirec, Cartraud, and Remacle (2003) with straight fibers is shown in Fig. 9 (b) and (c).
Elements that are cut by the boundary of a reinforcement volume are set to be x-elements. Those elements completely inside a reinforcement volume remain ordinary finite elements and are assigned with material properties of the fiber. Those outside the reinforcement volumes are ordinary elements as well but belong to the matrix material. In this vein element type and material allocation are determined for each element during the automated mesh generation process.
For defining the orientation of the material principal axis in the elements each of the reinforcement volumes is provided with an initial orientation. Variations from this configuration that occur in the course of crimped fibers are acquired from a moving trihedron whose direction is computed from the tangent vector of the fiber centerline and the initial state.

If the considered element turns out to be an x-element its domain is divided into material subspaces (Fig. 10 (a)). The common vertices of these material volumes form a discrete representation of the material interface

(a) CAD model of the reinforcing structure

(b) Overlay of regular X-FEM mesh

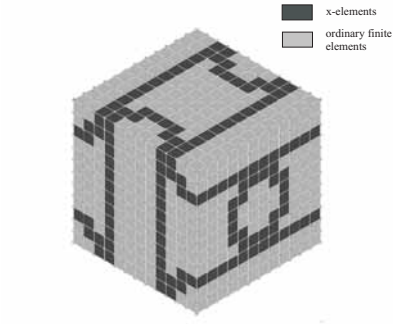

(c) Resulting regular X-FEM mesh

Figure 9 : Automated generation of a X-FEM mesh

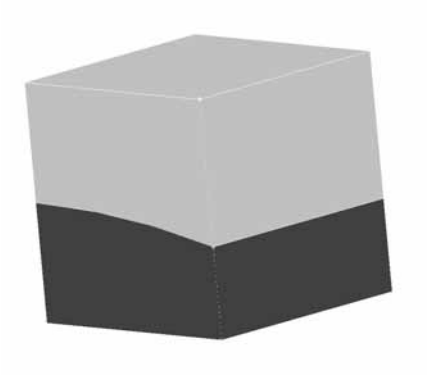

(a) Materials in the element domain

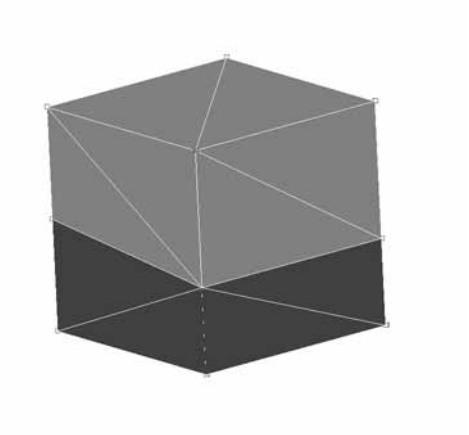

(b) Resulting DELAUNAY subdivision

Figure 10 : Element subdivision according to material sub-domains

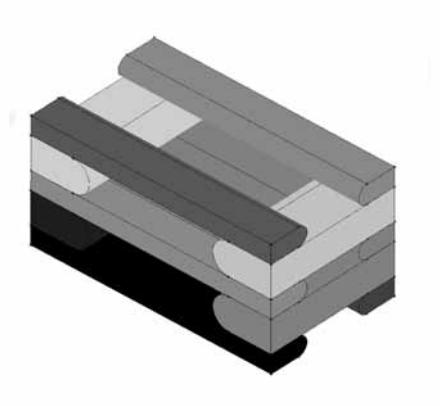

(a) Geometry model of reinforcement

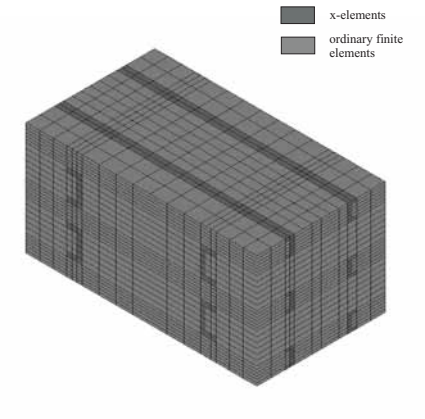

(b) X-FEM mesh

Figure 11 : Modelling of biaxial weft knit fabric

whose intersection with the element faces are straight lines.

In addition, these interface vertices and the nodes of the element are the input for the DELAUNAY hex-tet-subdivision creating tetrahedral integration spaces as it is illustrated in Fig. 10 (b). They are assigned with appropriate material properties for the integration process.

Now the values of the level-set-function φ_i at the element nodes - essential for the formulation of the enrichment function - are computed with respect to the interface resulting from the element subdivision. In this way it is possible to determine the level-set-values only at enriched nodes which saves numerical costs and facilitates the necessary distance computations.

Nevertheless, there is one hitch with level-set-representation of the interface computed on the element level. If a curved interface is approximated two adjacent elements provide different values of the level-set-function at joined nodes. Although the resulting approximation of the level-set-function $\varphi(\mathbf{x})$ is still continuous over the element boundary the displacement field will be discontinuous which might affect the convergence behavior of the problem.

On the other hand, averaging the level-set-function values at respective nodes which could ensure the desired continuity of the displacement field leads to a mismatch between the interpolation of φ and the boundaries of the integration tetrahedra. As a consequence the continuity of the integrand in each sub-domain cannot be guaranteed which might yield wrong integration results.

A biaxial glass epoxy fabric will be considered as example for the application of X-FEM to composite modelling. The geometry of the reinforcing structure in the

RVE is shown in Fig. 11 (a).

4.1.2 Example - biaxial fabric

Table 2 : Material parameters for yarn.

Parameter	E_1	E_2	E_3
Value	45.9 GPa	11.6 GPa	11.6 GPa
	G_{12}	G_{23}	G_{13}
	4.0 GPa	3.5 GPa	4.0 GPa
	ν_{12}	ν_{23}	ν_{13}
	0.3001	0.6677	0.3001

Table 3 : Comparison of effective macroscopic material parameters.

Parameter	**X-FEM**	FEM
$\overline{C}_{1111}$ [GPa]	19.8	19.5
$\overline{C}_{2222}$ [GPa]	20.2	20.3
$\overline{C}_{3333}$ [GPa]	11.7	11.7
$\overline{C}_{1122}$ [GPa]	6.4	6.4
$\overline{C}_{1133}$ [GPa]	6.9	6.9
$\overline{C}_{2233}$ [GPa]	6.9	6.9
$\overline{C}_{2323}$ [GPa]	1.9	1.9
$\overline{C}_{1313}$ [GPa]	2.0	2.0
$\overline{C}_{1212}$ [GPa]	2.0	2.0

Material parameters for warp and weft yarns are obtained from fiber and matrix properties using a rule of mixture. They are given in Tab. 2 with respect to the global coordinate system and characterize a transverse isotropic material behavior.

The matrix is isotropic with a Young's-Modulus of $E = 3.0$ GPa and a Poisson's ratio $\nu = 0.4$. Effective macroscopic stiffness parameters are sought after.

To this end the automated model generation procedure is used to create a X-FEM mesh for the RVE. From Fig. 11 (b) it can be observed that the resulting mesh in not completely regular. This is due to branching material interfaces in the model which cannot be treated with the defined x-element. A solution to this problem is in process and will remove this restriction.

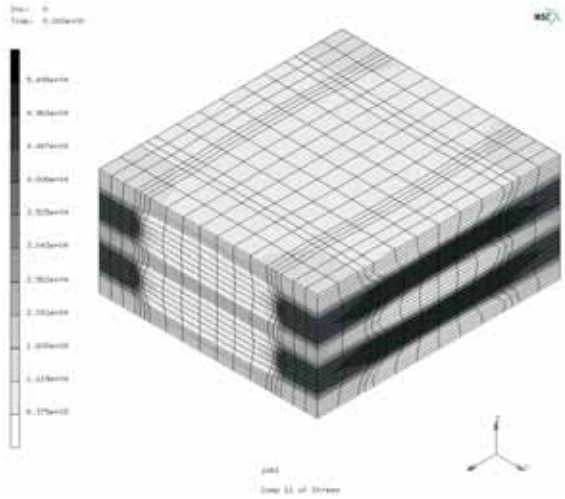

(a) Normal mode $\langle \varepsilon_{11} \rangle = 1$, plot shows σ_{11}

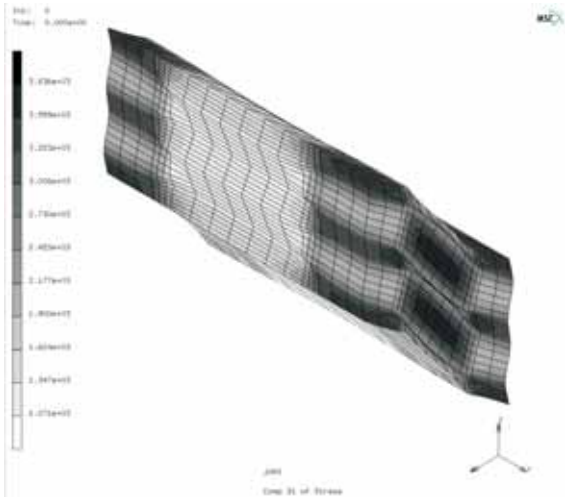

(b) Shear mode $\langle \varepsilon_{13} \rangle = 1$, plot shows σ_{13}

Figure 12 : Typical deformation modes

Eventually, periodic boundary conditions according to Eq. 13 are applied to the model including additional degrees of freedom at boundary nodes. Then each of the considered deformation modes is solved in MARC and mesoscopic stress fields are obtained. Fig. 12 shows the results for two typical deformation modes.

The desired effective stiffness properties are then computed by averaging these distributions. The resulting macroscopic material parameters are given in Tab. 3. A good agreement of the results received from the X-FEM model and a finite element reference solution is recognized. Furthermore, the ease of meshing of sharply tapered matrix domains between the fibers being a funda-

mental advantage of X-FEM over classical FEM modelling is noticed in this example.

4.2 The simulation of the tensile test

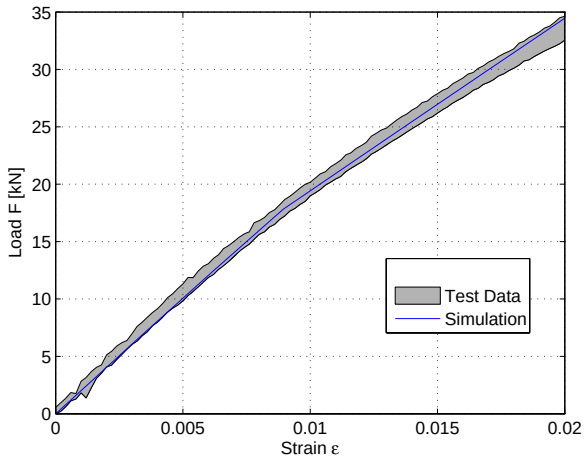

Figure 13 : Load-strain results

The macroscopic material behavior of textile reinforced composites and the results obtained by simulation procedures are verified by tensile tests. The dimensions of the specimen are as follows: length $l = 250$ mm; width $b = 50$ mm and thickness $d = 2.4$ mm. The demand for an uni-axial stress state requires a cross-sectional dimension of the specimen which is much smaller than the length. Due to the characteristic length scale of the reinforcement, the composite specimen cannot be defined according to such a criteria. Consequently, the stress and strain state over this rectangular specimen is neither homogeneous nor uni-axial. For this reason, a multi-scale simulation of the tensile test is verified by the test results. During the test procedure, a non-contacting laser extensometer is used to measure the change of the distance of two markers which are placed on the specimen surface in a distance of 50 mm. A strain value is computed based on the initial distance of these markers. Five specimens with one particular orientation of the textile reinforcement are tested. Variations can be found between the sets of measuring data. These are caused by e.g. a fluctuating orientation of the textile reinforcement. Hence the grey filled area in Fig. 13 represents the range of the load-strain relations obtained by the experimental tests.
The results of an test-equivalent simulation is depicted in the same diagram. A good agreement can be found comparing test and simulation results.

4.3 The elevator bucket

Buckets as shown in Fig. 14 are the essential components of a conveyor which is used to elevate certain materials. Conventionally, the buckets are made of steel. However,

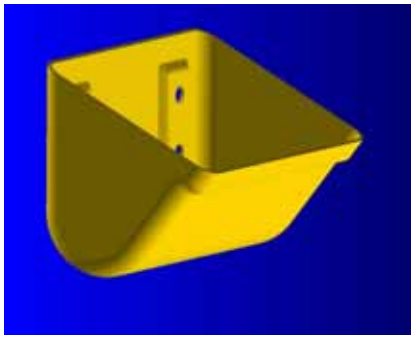

Figure 14 : Elevator bucket

a non-metallic bucket has several advantages such as: (i) the lightweight mode of the construction, (ii) the chemical resistance and (iii) the food-compatibility.
In Fig. 15 a picture of the textile preform is presented. The grid of black lines emphasizes the orientation and shear deformation due to the draping process. The development of a FE-model can be subdivided into following steps:

1. To generate the geometry of the structural part in the FE-preprocessor an standard interface to a CAD-program is used.

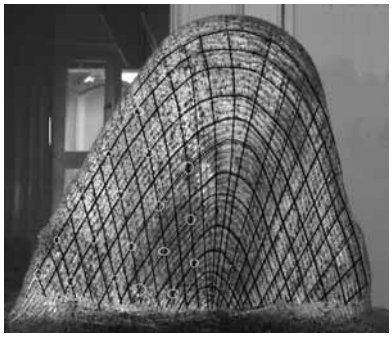

Figure 15 : Textile preform

2. The surface data and the location of the grid points shown in Fig. 15 are evaluated by the 3D optical measuring system ARAMIS.

3. The data measured by ARAMIS are integrated into the FE-preprocessor. The related surfaces are subdivided according to the grid points.

4. After the generation of the FE-mesh each finite element can be associated to a certain area. This in turn defines the global orientation and the shear deformation of the textile reinforcement. With the help of the user-subroutine *usermat* provided by the UPF's, the material properties are computed based on the procedure outlined in section 3.1 and the principle directions are adjusted.

To verify the results of this modelling and simulation strategy, experimental investigations are performed. For this, a bucket is filled with steel balls whose total weight amounts 60 kg. The deformation caused by this load is measured by ARAMIS. The boundary conditions of the FE-model are defined according to the experimental set-up. Due to the symmetry in the construction and the load, it is sufficient to consider a half of the bucket, only. In Fig. 16, the FE-model is shown. The color scale

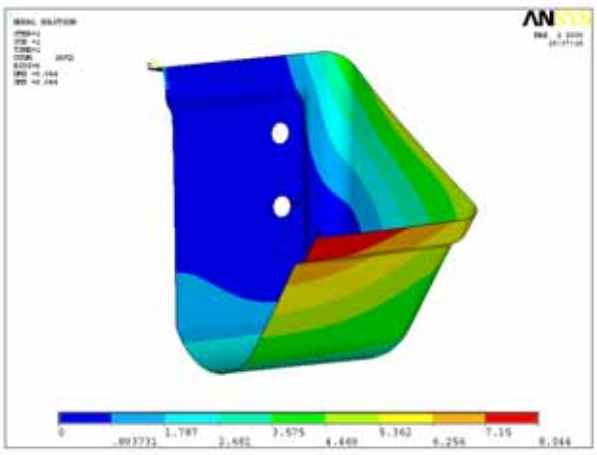

Figure 16 : FE-model of the elevator bucket

is adjusted according to the total displacement. The diagram shown in Fig. 17 compares a displacement measured by ARAMIS and computed by the FE-simulation. The two curves in this graph represent the total displacement along the cutting edge of the bucket. The very good

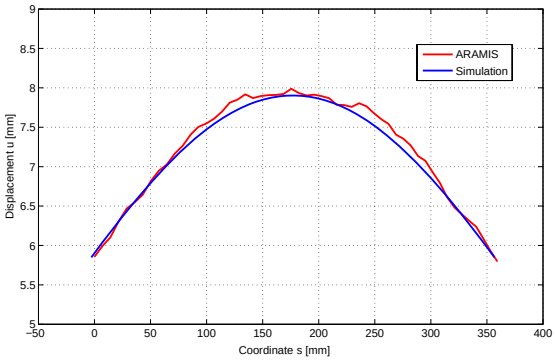

Figure 17 : Verification of the total displacement

agreement of these results demonstrate the usability of this procedure.

5 CONCLUSION

A multi-scale homogenization procedure as well as a new x-element formulation are implemented into commercial FE-programs. The successful application of two different modelling strategies - Binary Model and X-FEM - to complex structured composite materials demonstrates their usability and advantages.
However, there is still a lot of work to be done in order to advance the flexibility, performance and reliability of these methods. Related current research is addressed to following problems:

- The computational multi-scale procedure demands for extremely high numerical power to reduce the computational time. This can be achieved e.g. by the enhanced performance of multi-processor technology.

- Already under small load or deformation most composite materials exhibit a non-linear material behavior. Further research is required to analyze and implement these processes into the modelling and simulation strategies.

- The generation of a model representing a composite with any reinforcing architecture in the frame work of the X-FEM without adaptation of the regular mesh requires a x-element formulation including two material boundary surfaces.

Acknowledgement: The work done for this paper is sponsored by the German Research Community (DFG) in the context of the priority program (SPP) no. 1123 and the collaborative research center (SFB) no. 639.

References

Ansys (2004): Guide to ansys user programmable features- ansys release 9.0, 2004.

Atluri, S. N.; Shen, S. (2005): The basis of meshless domain discretization: the meshless local petrov–galerkin (mlpg) method. *Advances in Computational Mathematics*, vol. 23, no. 1 - 2, pp. 73–93.

Belytschko, T.; Black, T. (1999): Elastic crack growth in finite elements with minimal remeshing. *International Journal for Numerical Methods in Engineering*, vol. 45, no. 5, pp. 601–620.

Belytschko, T.; Moës, N.; Usui, S.; Parimi, C. (2001): Arbitrary discontinuities in finite elements. *Int. J. Numer. Meth. Engng.*, vol. 50, pp. 993–1013.

Carter, W.; Cox, B.; Fleck, N. (1994): A binary model of textile composites - i. formulation. *Acta metall. mater.*, vol. 42, no. 10, pp. 3463–3479.

Carter, W.; Cox, B.; McGlockton, M.; Xu, J. (1995): A binary model of textile composites - ii. the elastic regime. *Acta metall. mater.*, vol. 43, no. 9, pp. 3511–3524.

Diestel, O.; Haasemann, G.; Orawattanasrikul, S. (2004): Biaxialgestrickpreformen mit komplexer geometrie, experimentelle untersuchung und simulation der verbundeigenschaften. *ITB-Mitteilungen*, vol. 2, pp. 19–27.

Hill, R. (1972): On constitutive macro-variables for heterogeneous solids at finite strain. *Proc. R. Soc. Lond. A*, vol. 326, no. 1565, pp. 131–147.

Holmbom, A.; Persson, L.; Svanstedt, N. (1991): A homogenization procedure for computing effective moduli and microstresses in elastic composite materials. *Composite Engineering*, vol. 2, no. 4, pp. 249–259.

Kouznetsova, V. (2002): *Computational homogenisation for the multi-scale analysis of multi-phase materials*. PhD thesis, TU Eindhoven, 2002.

Kwon, Y. W.; Roach, K. (2004): Unit-cell model of 2/2-twill woven fabric composites for multi-scale analysis. *CMES: Computer Modeling in Engineering & Sciences*, vol. 5, no. 1, pp. 63–72.

Melenk, J.; Babuška, I. (1996): The partition of unity finite element method: Basic theory and applications. Research Report 96-01, Eidgenssische Technische Hochschule- Zrich, 1996.

Miehe, C.; Koch, A. (2002): Computational micro-to-macro transitions of discretized microstructures undergoing small strains. *Arch. Appl. Mech.*, vol. 72, pp. 300–317.

Moës, N.; Cloirec, M.; Cartraud, P.; Remacle, J. (2003): A computational approach to handle complex microstructure geometries. *Comput. Method. Appl. M.*, vol. 192, pp. 3163–3177.

Moës, N.; Dolbow, J.; Belytschko, T. (1999): A finite element method for crack growth without remeshing. *Int. J. Numer. Meth. Engng.*, vol. 46, pp. 131–150.

Sladek, V.; Sladek, J.; Tanaka, M. (2005): Local integral equations and two meshless polynomial interpolations with application to potential problems in non-homogeneous media. *CMES: Computer Modeling in Engineering & Sciences*, vol. 7, no. 1, pp. 69–84.

Sukumar, N.; Chopp, D.; Moës, N.; Belytschko, T. (2001): Modeling holes and inclusions by level sets in the extended finite element method. *Comput. Methods Appl. Mech. Engrg.*, vol. 190, pp. 6183–6200.